ACS APPLIED MATERIALS & INTERFACES

www.acsami.org
Research Article

Transition Temperature-Guided Design of Lipid Nanoparticles for Effective mRNA Delivery

Jeong Eun Shin, Eun-jeong Won, Junchao Xu, Jong Cheol Lee, Jeong Kyu Bang,*,# Michael J. Mitchell,*,# and Hyunjoo Cha-Molstad*,#

Cite This: ACS Appl. Mater. Interfaces 2025, 17, 28012−28024
Read Online

ACCESS | Metrics & More | Article Recommendations | Supporting Information

ABSTRACT: Lipid nanoparticles (LNPs) are promising mRNA delivery vehicles due to their biocompatibility and tunable characteristics. While current rational design approaches focus on ionizable lipids' pK_a and zeta potential to optimize mRNA encapsulation and endosomal escape, the selection of helper lipids remains largely empirical. We propose that the lipid transition temperature (T_m), marking the shift from the gel to the liquid crystalline phase, can guide rational helper lipid selection. Through screening 54 ionizable lipids, we identified H7T4, which displayed favorable physicochemical properties when combined with its tail variants but exhibited poor transfection efficiency. Using nano differential scanning calorimetry (nDSC) and biological small-angle X-ray scattering (BioSAXS), we found that lowering the system's T_m by combining H7T4 (high transition temperature) with a low-transition-temperature helper lipid such as 1,2-dioleoyl-*sn*-glycero-3-phosphoethanolamine (DOPE) significantly enhanced mRNA cellular uptake both *in vitro* and *in vivo*. These findings establish T_m as a crucial parameter for a rational LNP design.

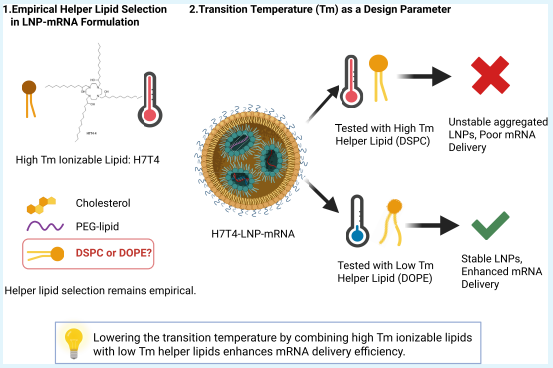

KEYWORDS: *mRNA, lipid nanoparticle, nDSC, SAXS, ionizable lipid*

INTRODUCTION

The advent of mRNA-based therapeutics has transformed biotechnology and medicine, promising novel treatments for various diseases.[1,2] This advancement stems from the development of efficient delivery systems capable of protecting and delivering mRNA into target cells. Lipid nanoparticles (LNPs) are the most favorable candidates for nucleic acid delivery because of their clinical success in COVID-19 mRNA vaccines and the ease of manipulating the size, composition, surface modification, and high biocompatibility.[1−4]

LNPs comprise ionizable lipids, helper lipids, cholesterol, and PEG-lipids.[5,6] Among the lipid components, ionizable lipids are the most critical to LNP performance because they contribute to both mRNA loading into LNPs and the endosomal escape of mRNA into the cytoplasm.[7−9] These lipids are designed to transition between different ionization states in response to changes in pH, which is essential for overcoming the endosomal membrane and achieving effective mRNA delivery.[10,11] Under the acidic pH of late endosomes, ionizable lipids become positively charged, facilitating the efficient release of mRNA from endosomes while remaining neutral in physiological pH conditions.[12−14]

The behavior of ionizable lipids under varying conditions, including pH, significantly influences their performance in LNP systems.[15,16] One critical parameter is the transition temperature of the lipid.[17] This temperature marks the point at which the lipid phase changes from a gel-ordered state with tightly packed alkyl chains to a liquid crystalline state where the alkyl chains become disordered.[18,19] In a liquid crystalline state, the lipid can be easily manipulated to form nanoparticles of smaller sizes.[20] This transition temperature is influenced by several factors, including the nature of the lipid headgroups,[17] alkyl tail saturation,[21] and chain length.[22−24] Therefore, the transition temperature is used to predict lipid inter- and intramolecular interactions and their effects on lipid self-assembly into nanoparticles and stability during storage and administration.[25,26]

Despite advances in LNP design focusing on ionizable lipids, the selection of helper lipids remains a trial-and-error process, often leading to suboptimal delivery efficiency and reproducibility issues.[27−33] Each ionizable lipid has an optimal combination of helper lipids that enables the formation of stable lipid nanoparticles and the most efficient nucleic acid

Received: March 31, 2025
Revised: April 21, 2025
Accepted: April 27, 2025
Published: May 6, 2025

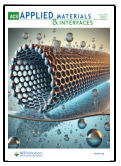

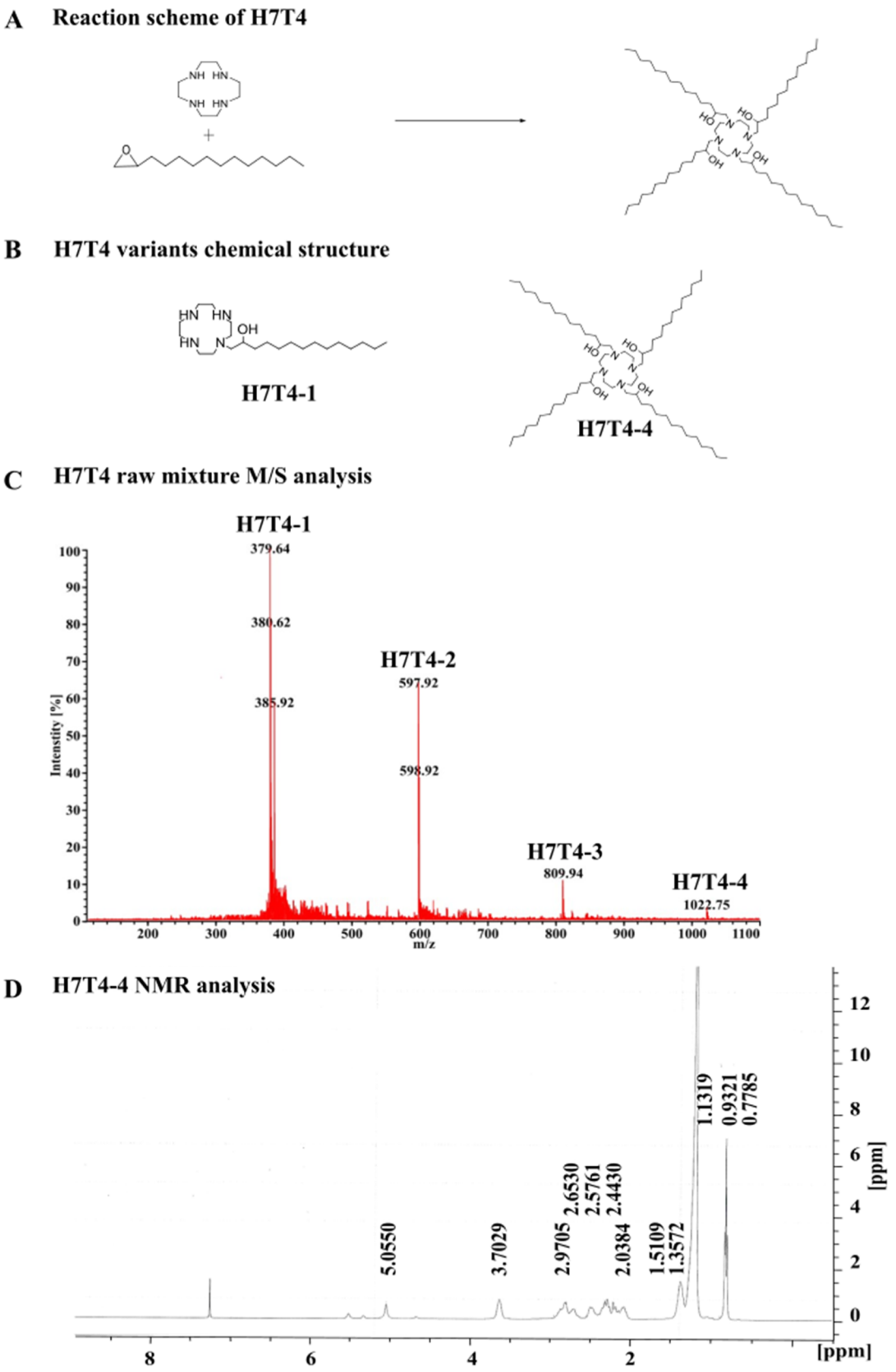

Figure 1. Synthesis, characterization, and spectroscopic analysis of H7T4: MS and NMR studies of raw lipid reaction products. (A) Reaction scheme and chemical structure of H7T4. (B) Chemical structures of H7T4 variants (left: H7T4−1; right: H7T4−4). (C) Mass spectra of H7T4 raw mixture. (D) NMR data of pure H7T4−4.

delivery.[5,6,34−38] For example, Moderna's ionizable lipid, SM-102, showed optimal storage and transfection performance with DSPC,[39,40] while C12−200 combined with DOPE induced higher protein expression than when combined with

https://doi.org/10.1021/acsami.5c06464
ACS Appl. Mater. Interfaces 2025, 17, 28012−28024

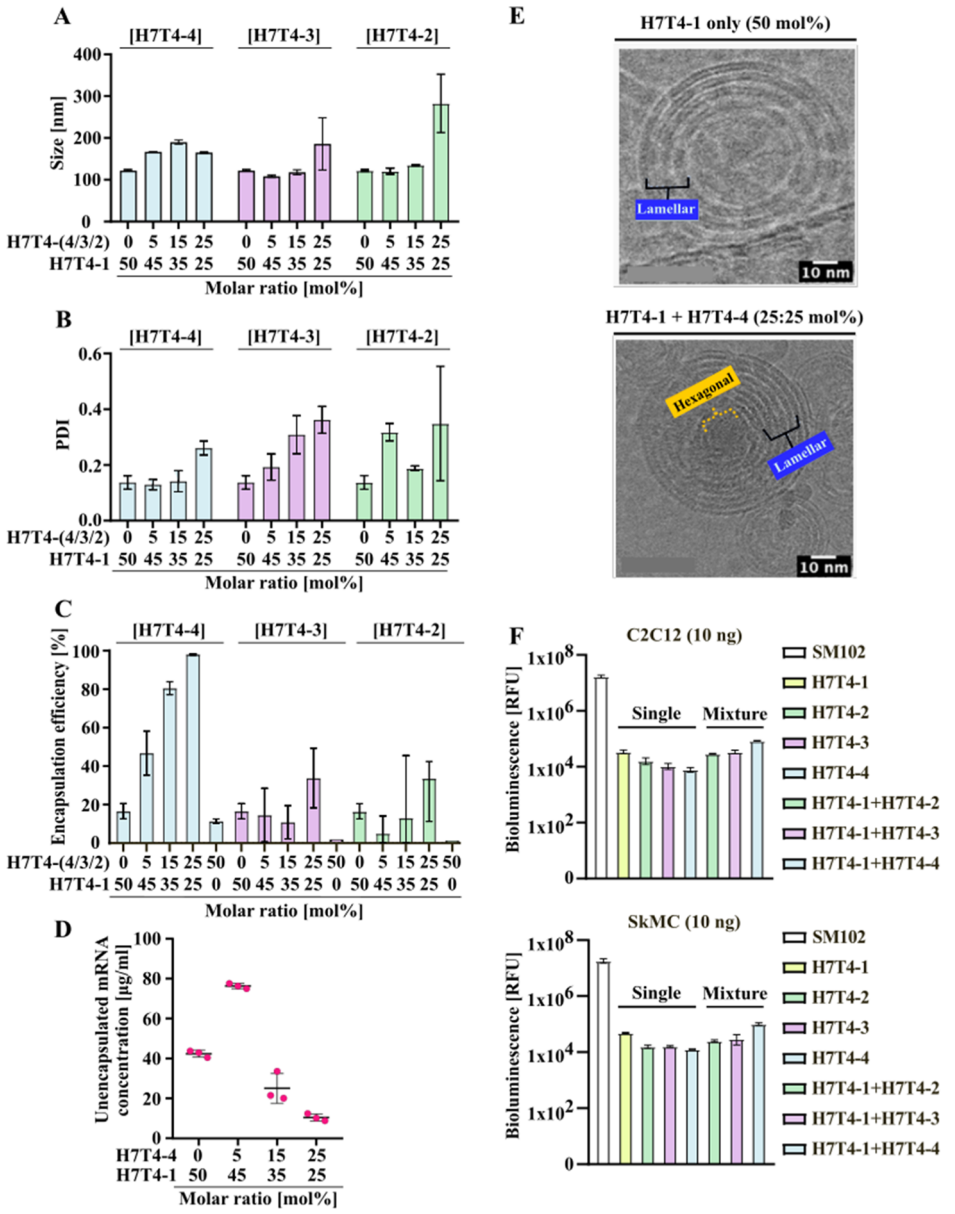

Figure 2. Characterization of LNPs with H7T4 variants. (A) Sizes of LNPs using H7T4 variants with different tail numbers. (B) PDIs of LNPs using H7T4 variants with different tail numbers. (C) Encapsulation efficiencies of LNPs with H7T4 variants. (D) Unencapsulated mRNA concentrations post-LNP formulation with H7T4 variant. (E) Cryo-TEM for H7T4−1 only LNPs H7T4−1/DSPC/cholesterol/PEG-lipid (50/10/38.5/1.5 mol %) and H7T4−1 + H7T4−4 LNPs H7T4−1/H7T4−4/DSPC/cholesterol/PEG-lipid (25/25/10/38.5/1.5 mol %). Cryo-TEM analysis followed dialysis against PBS to remove ethanol (pH 4.5) and neutralize the LNPs (pH 7.4). Scale bar = 100 nm. (F) *In vitro* firefly luciferase assays (n = 3, biologically independent samples). LNPs were formulated with H7T4 variant(s)/DSPC/cholesterol/PEG-lipid (50/10/38.5/1.5 mol %), using either single H7T4 variants or H7T4 variant combinations in equal proportions (25:25 mol %). Two muscle cell lines (C2C12 and SkMC) were treated with firefly luciferase mRNA-loaded H7T4 LNPs at a 10 ng/well mRNA dose for 24 h. Data are represented as mean ± SD.

DSPC.[41−43] Until now, the optimal combination has been determined through empirical trial and error. By introducing the lipid transition temperature (T_m) as a guiding parameter, our study aims to provide a rational framework for helper lipid selection, potentially enhancing the efficacy of mRNA delivery systems.

In this study, we describe the synthesis of a new series of ionizable lipids with tailored properties to enhance the delivery of mRNA. Our synthetic strategy focuses on designing ionizable lipids with specific structural features that optimize their performance in LNP formulations. Following synthesis, we investigated the transition temperature of these lipids using nano differential scanning calorimetry (nDSC)[44−48] and other relevant methods. This analysis provided insights into their thermal properties and influence on the formation of stable and functional LNPs. Our new ionizable lipid, H7T4, exhibits strong intermolecular interactions due to its cyclic headgroup and four hydrophobic alkyl tails, resulting in a high transition temperature.[49,50] Therefore, H7T4 did not form stable lipid nanoparticles (LNPs) with helper lipids that have high transition temperatures, such as DSPC. However, successful mRNA/LNP formation was achieved with helper lipids having relatively lower transition temperatures, such as DOPE, with a

https://doi.org/10.1021/acsami.5c06464
ACS Appl. Mater. Interfaces 2025, 17, 28012−28024

notable decrease in the transition temperature observed in these H7T4-DOPE formulations.

Our findings reveal the critical relationship between the transition temperature and lipid performance in LNP-based mRNA delivery systems, providing specific strategies for optimizing LNP formulations. For ionizable lipids with high transition temperatures, stable LNPs can be formed by selecting helper lipids with relatively lower transition temperatures to facilitate component mixing and by reducing the ionizable lipid ratio to 20−25% from the conventional 35−50% used in approved products. This work establishes new design principles for ionizable lipids in mRNA-LNP formulations, advancing the development of more effective and reliable mRNA-based therapeutics.

RESULTS AND DISCUSSION

Synthesis and Characterization of an Ionizable LNP Library. A library of 54 ionizable lipids was synthesized by using Michael addition chemistry. Alkyl tails are designated by tail length: *A* = C12, *B* = C14, and *C* = C16 were reacted with polyamine molecules (labeled numerically 1 through 18) to form polyamine-lipid cores. These ionizable lipids were combined with cholesterol, DMG-PEG, and helper lipid [1,2-distearoyl-*sn*-glycero-3-phosphocholine (DSPC)] at a molar ratio of 50:38.5:1.5:10 (ionizable lipid/cholesterol:DMG-PEG:DSPC). The lipid mixture was formulated to encapsulate eGFP or firefly luciferase mRNA using pipetting or a herringbone-style microfluidic device (Figure S1).

The manufactured LNP formulations were characterized for their particle size (hydrodynamic diameter), size distribution (polydispersity index, PDI), and surface charge (zeta potential) using a Zetasizer nano. In this library, LNP size ranged from 94.4 to 336.4 nm, with PDI ranging from 0.082 to 0.427. For effective intracellular delivery, nanoparticles typically require sizes between 10 and 200 nm and PDI values less than 0.2. Based on these criteria, we selected LNPs synthesized from 12 different polyamines that demonstrated both small size (hydrodynamic diameter <200 nm) and relative monodispersity (PDI <0.2). From the initial library, LNPs with 4 different polyamines as head groups were excluded due to low encapsulation efficiencies (<80%).

After the first screening of the LNP library through physical characterization, we evaluated mRNA transfection efficiency by performing reporter gene (eGFP or firefly luciferase) assays in HEK293T cells 24 h after treatment (Figure S2).[9,51] We evaluated the percentage of GFP-positive cells indicative of each LNP's mRNA delivery efficiency. Each ionizable lipid formulation demonstrated distinct levels of delivery efficiency, highlighting the critical role of an ionizable lipid structure in mRNA delivery (Figure S2).

One-Pot Synthesis of H7T4 Predominantly Yielded Single-Tailed H7T4−1. Based on the library screening, we identified H7T4, synthesized from cyclen tetrahydrochloride and 1,2-epoxytetradecane (C14), as a promising candidate for further investigation in LNP formulation optimization. The cyclen tetrahydrochloride core contains four secondary amines, allowing the attachment of up to four alkyl tails (Figure 1A,B).

The intracellular delivery of nucleic acids such as mRNA requires an efficient endosomal escape, a process crucially facilitated by the inverse hexagonal phase structure of ionizable lipids.[12,13,52−54] This structure enables ionizable lipids to efficiently disrupt endosomal membranes, allowing the cargo to escape into the cytoplasm and exert its therapeutic effect.[55] We hypothesized that the transition to an inverse hexagonal phase could be enhanced by increasing the alkyl tail number, which would result in a larger hydrophobic volume relative to the headgroup. To test this hypothesis with H7T4, we synthesized and purified variants with different numbers of alkyl tails. The structure of each H7T4 variant was confirmed by mass spectral analysis and NMR (Figures 1D and S3−S6). H7T4−4, comprising cyclen tetrahydrochloride with four alkyl tails, was initially formulated into LNPs with cholesterol, DSPC, and DMG-PEG since it has the maximum tail number. However, physicochemical analysis revealed that unlike the crude H7T4 mixture, the H7T4−4 LNP formulation failed to form stable nanoparticles (Figure 2A−C). This discrepancy prompted us to analyze unpurified H7T4 using mass spectrometry (Figure 1C), which revealed that it contained four distinct variants with different numbers of alkyl tails. After purification, the relative amounts in the final mixture were approximately 90% one-tailed variants and less than 1% four-tailed variants, with the remaining portion consisting of two- and three-tailed variants.

Four-Tail H7T4−4 Successfully Encapsulated mRNA Only When Mixed with Single-Tailed H7T4−1. Since the unpurified H7T4 mainly contained H7T4−1 (cyclen tetrahydrochloride with a single tail) and showed some luciferase expression, we hypothesized that H7T4−1 should be responsible for the observed transfection efficiency. However, H7T4−1 alone would likely be insufficient for effective endosomal escape, as its single hydrophobic tail may not provide adequate membrane-disrupting capability. This suggests that the observed transfection efficiency results from the cooperative action of H7T4−1 with other H7T4 tail variants present in the mixture rather than that of H7T4−1 alone. Therefore, we mixed H7T4−1 with other H7T4 alkyl tail variants (H7T4−2, H7T4−3, and H7T4−4) and assessed LNP size and PDI for formulations with different H7T4 variant combinations and ratios (Figure 2A,B). Interestingly, only the H7T4−1/H7T4−4 combination formed uniform LNPs (<200 nm) with PDI <0.3 across all ratios. In contrast, other variant combinations produced large (>600 nm), highly aggregated particles with significant size heterogeneity. Next, we investigated the mRNA encapsulation efficiency of LNPs formulated with various H7T4 variant combinations using the RiboGreen assay.[56] Results showed that only the H7T4−1/H7T4−4 combination achieved mRNA encapsulation efficiency >90% at 25:25 mol %, while other combinations failed to do so (Figure 2C). Notably, the encapsulation efficiency of the H7T4−1/H7T4−4 combination increased from 20% to 90% as the H7T4−4 ratio increased from 0 to 25 mol % (Figure 2C). Consistently, free mRNA concentration decreased linearly from 40 to 10 μg/mL as the H7T4−4 proportion increased from 5 to 25 mol % (Figure 2D), suggesting that H7T4−4 plays a crucial role in mRNA encapsulation.

We then employed cryo-TEM imaging to investigate the morphology and internal structure of LNPs containing either the H7T4−1/H7T4−4 (25:25 mol %) combination or H7T4−1 alone. The cryo-TEM images revealed spherical particles and provided insights into their internal structure: LNPs containing the H7T4−1/H7T4−4 combination showed organized lipid lamellar bilayers and solid core hexagonal structures, whereas LNPs containing H7T4−1 alone lacked core materials (Figure 2E).[57,58]

https://doi.org/10.1021/acsami.5c06464
ACS Appl. Mater. Interfaces 2025, 17, 28012−28024

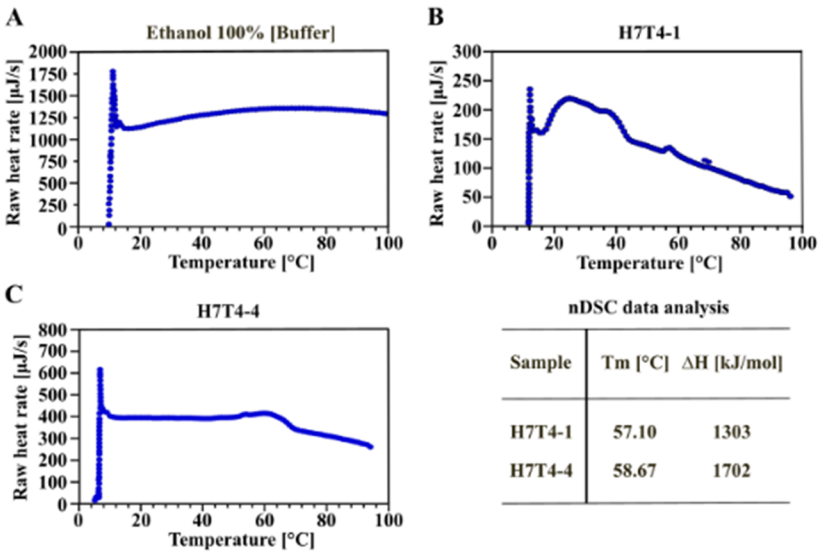

Figure 3. nDSC thermograms of H7T4 variants. Nano differential scanning calorimetry (nDSC) thermograms of (A) buffer (ethanol 100%) and H7T4 variants (B: H7T4−1 and C: H7T4−4) were obtained to characterize the phase transition of lipids as a function of temperature. The transition temperature of H7T4 variants is indicated as T_m, and enthalpy changes during phase transition, as ΔH.

Finally, we examined the transfection efficiency of LNPs containing either single H7T4 or H7T4 variant combinations. As expected, LNPs containing either single H7T4 variants or H7T4 variant combinations with low encapsulation efficiency showed negligible transfection efficiency compared with the SM-102 LNP control. Notably, even LNPs containing the H7T4−1/H7T4−4 combination, which demonstrated high encapsulation efficiency and uniform size distribution, displayed significantly low transfection efficiency compared to SM-102, indicating that favorable physicochemical properties do not necessarily translate into high transfection efficiency (Figure 2F).

Single-Tailed H7T4−1 Helped Moderate Four-Tail H7T4−4's Strong Intermolecular Interactions. Despite the promising physical characteristics of LNPs formulated with the H7T4−1/H7T4−4 combination, their poor transfection efficiency prompted us to investigate the underlying mechanisms. According to Figure 2C,D, H7T4−4 appears to function like typical ionizable lipids in mRNA encapsulation, as its increasing ratio relative to H7T4−1 correlates with higher encapsulation efficiency and lower free mRNA concentration, peaking when H7T4−4 comprises 25 mol % of the mRNA/LNP formulation. H7T4−1, with a single alkyl tail, lacks sufficient hydrophobic interactions to effectively encapsulate mRNA on its own (Figure 2C). In contrast, H7T4−4, possessing four alkyl tails, exhibits strong hydrophobic interactions but may form rigid structures that hinder mRNA/LNP formation. When combined, H7T4−1 may act as a molecular spacer, reducing the rigidity imparted by H7T4−4 and facilitating better lipid mixing and mRNA encapsulation.

To better understand this physical relationship between H7T4−1 and H7T4−4, we investigated their thermodynamic properties (transition temperatures and enthalpy changes) using nano differential scanning calorimetry (nDSC), as these properties might drive phase separation and domain formation during mRNA/LNP formulation. The transition temperature (the temperature at which lipids undergo a phase transition, typically from a gel phase to a liquid phase or vice versa[55]) can affect lipid mixing during mRNA/LNP formulations. Lipid transition temperatures are influenced by several structural features. Longer acyl chains increase transition temperatures due to stronger van der Waals interactions,[22−24] while unsaturated or branched chains lower them by reducing packing efficiency.[21] The chemical nature of the lipid headgroup can also affect the transition temperature. Larger noncyclic and more polar headgroups tend to have lower transition temperatures,[59,60] while cyclic headgroups increase transition temperatures by enhancing packing efficiency, creating stronger intermolecular interactions, and increasing molecular rigidity, collectively resulting in more stable, densely packed bilayers that require higher energy for phase transitions.[61,62]

Our nDSC analysis revealed transition temperatures of 57.1 °C for H7T4−1 and 58.6 °C for H7T4−4 (Figure 3B,C, and table), higher than those of other ionizable or helper lipids.[44−48] 100% ethanol (used as a buffer) served as a reference control (Figure 3A). These data suggest that the shared cyclic amine head, being the common structural feature between the variants, is primarily responsible for their high transition temperatures, while their different tail structures play a crucial role in mRNA/LNP formation. When mixed at an equal molar ratio, H7T4−1's single tail with lower packing efficiency helps moderate the strong intermolecular interactions caused by H7T4−4's four tails with large hydrophobic volume, enabling stable mRNA/LNP formation.

Mixing H7T4−4 with Low-Transition-Temperature Helper Lipids Decreased Overall T_m and Greatly Enhanced Transfection Efficiency. High transition temperatures could result in more rigid lipid bilayers, which impede both mRNA/LNP formation and the necessary conformational changes and membrane fusion events required for efficient cell entry and endosomal escape. Even when mRNA/LNP is successfully formed, this reduced membrane fluidity could hinder the ability of these complexes to interact with cellular and endosomal membranes. Consequently, formulations with high T_m lipids such as H7T4−4 and DSPC exhibit poor mRNA encapsulation efficiency. Notably, our previous formulation (H7T4−1/H7T4−4/DSPC/cholesterol/PEG-lipid at 25/25/10/38.5/1.5 mol %), despite achieving high encapsulation efficiency, showed negligible transfection

https://doi.org/10.1021/acsami.5c06464
ACS Appl. Mater. Interfaces 2025, 17, 28012−28024

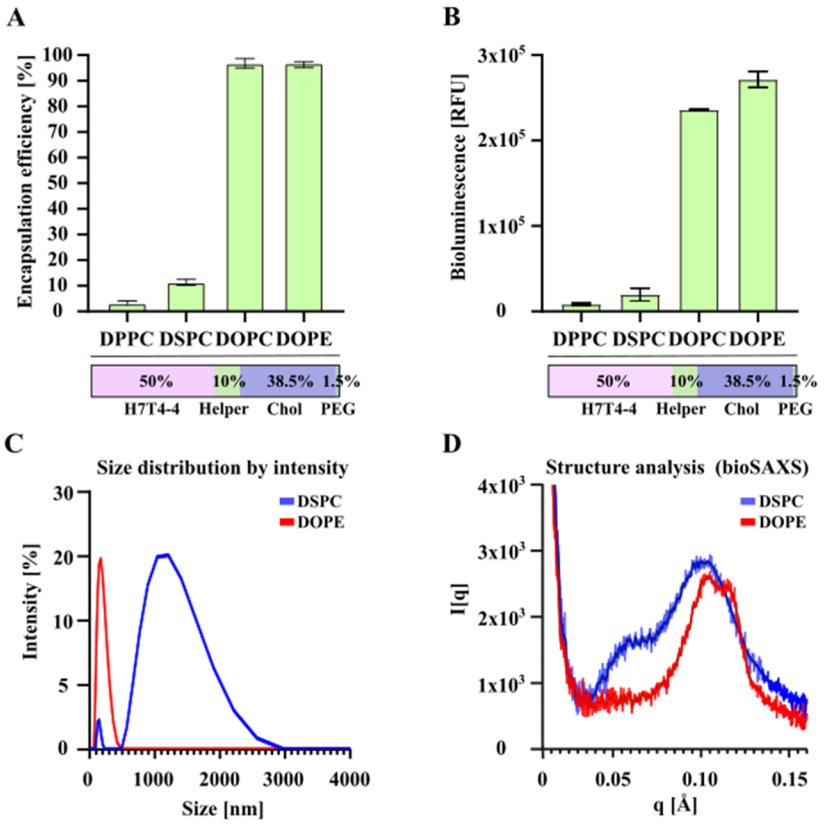

Figure 4. Characterization of H7T4−4 LNPs with other helper lipids. (A) Encapsulation efficiency of H7T4−4 LNPs with different helper lipids (H7T4−4/helper lipid/cholesterol/PEG-lipid at 50/10/38.5/1.5 mol %). (B) *In vitro* mRNA delivery of H7T4−4 LNPs with different helper lipids in C2C12 cells. (C) Size distribution data for H7T4−4 LNPs with different helper lipids. (D) SAXS data for H7T4−4 LNPs with different helper lipids SAXS data for H7T4 lipid variants. To accommodate the SAXS data, each set was given an offset (empty: 0.2 and POPC-TO: 1 unit).

efficiency (Figure 2F). This poor performance likely stems from the high transition temperatures of both the ionizable lipids (H7T4−1 and H7T4−4) and the helper lipid (DSPC). To test this hypothesis, we prepared LNPs combining H7T4−4 with four distinct helper lipids: two with high T_m (DPPC and DSPC) and two with low T_m (DOPC and DOPE), where DPPC is 1,2-dipalmitoyl-*sn*-glycero-3-phosphocholine, DSPC is 1,2-distearoyl-*sn*-glycero-3-phosphocholine (DSPC), DOPC is 1,2-dioleoyl-*sn*-glycero-3-phosphocholine, and DOPE is 1,2-dioleoyl-*sn*-glycero-3-phosphoethanolamine. As predicted, H7T4−4 alone (50 mol %) formed functional mRNA/LNPs with low-transition-temperature helper lipids (DOPC and DOPE) that successfully transfected mRNA but failed to form effective mRNA/LNPs with high-transition-temperature helper lipids (DPPC and DSPC) (Figure 4A,B).

Dynamic light scattering measurements revealed a single narrow peak at 100 nm when H7T4−4 was combined with the DOPC, indicating the formation of small, uniform LNPs. In contrast, formulation with DPPC showed a bimodal distribution with peaks at around 100 and 1000 nm, suggesting particle aggregation (Figure 4C).

We then employed small-angle X-ray scattering (SAXS) to examine the nanoscale structural characteristics of H7T4−4 LNPs.[63,64] H7T4−4/DOPE LNPs showed distinct, well-defined peaks at $q \sim 0.10$ in the SAXS profile, indicating monodisperse particles of ∼100 nm. In contrast, H7T4−4/DSPC LNPs exhibited multiple peaks ($q \sim 0.10$, 0.05, and 0.03) (Figure 4D), consistent with the presence of larger aggregates observed by DLS.

The thermodynamic properties of lipids, particularly their phase behavior and ability to form mixed phases, are governed by the molecular structure. Lipids with high transition temperatures often exhibit stronger intermolecular interactions, making them thermodynamically unfavorable to mix with other lipids.[65]

When H7T4−4 is combined with high-transition-temperature lipids (DSPC: T_m = 55 °C and DPPC: T_m = 41 °C), phase separation occurs, preventing stable mRNA/LNP formation. In contrast, low-transition-temperature lipids (DOPE: T_m = −16 °C and DOPC: T_m = −17 °C) exhibit greater molecular mobility, enabling H7T4−4 to mix effectively with other components such as cholesterol and DMG-PEG, leading to the formation of stable mRNA/LNPs capable of efficient mRNA delivery.

These findings highlight how lipid transition temperature and molecular compatibility critically influence membrane dynamics, LNP formulation, and ultimately transfection efficiency.

Optimized H7T4 LNPs Demonstrated Efficient mRNA Delivery *In Vitro* and *In Vivo*. We further optimized the H7T4−4 LNP formulation using DOPE as a miscible helper lipid. Through systematic reduction of the H7T4−4 content from 50 to 10 mol %, we determined that 20 mol % H7T4−4 achieved maximal *in vitro* mRNA delivery. Further optimization of cholesterol, DOPE, and DMG-PEG 2000 ratios led to the final optimal formulation: H7T4−4/DOPE/cholesterol/DMG-PEG 2000 (20/41/38/1 mol %) (Figure 5A). The lower ionizable lipid content in H7T4 LNPs (20 mol %)

https://doi.org/10.1021/acsami.5c06464
ACS Appl. Mater. Interfaces 2025, 17, 28012−28024

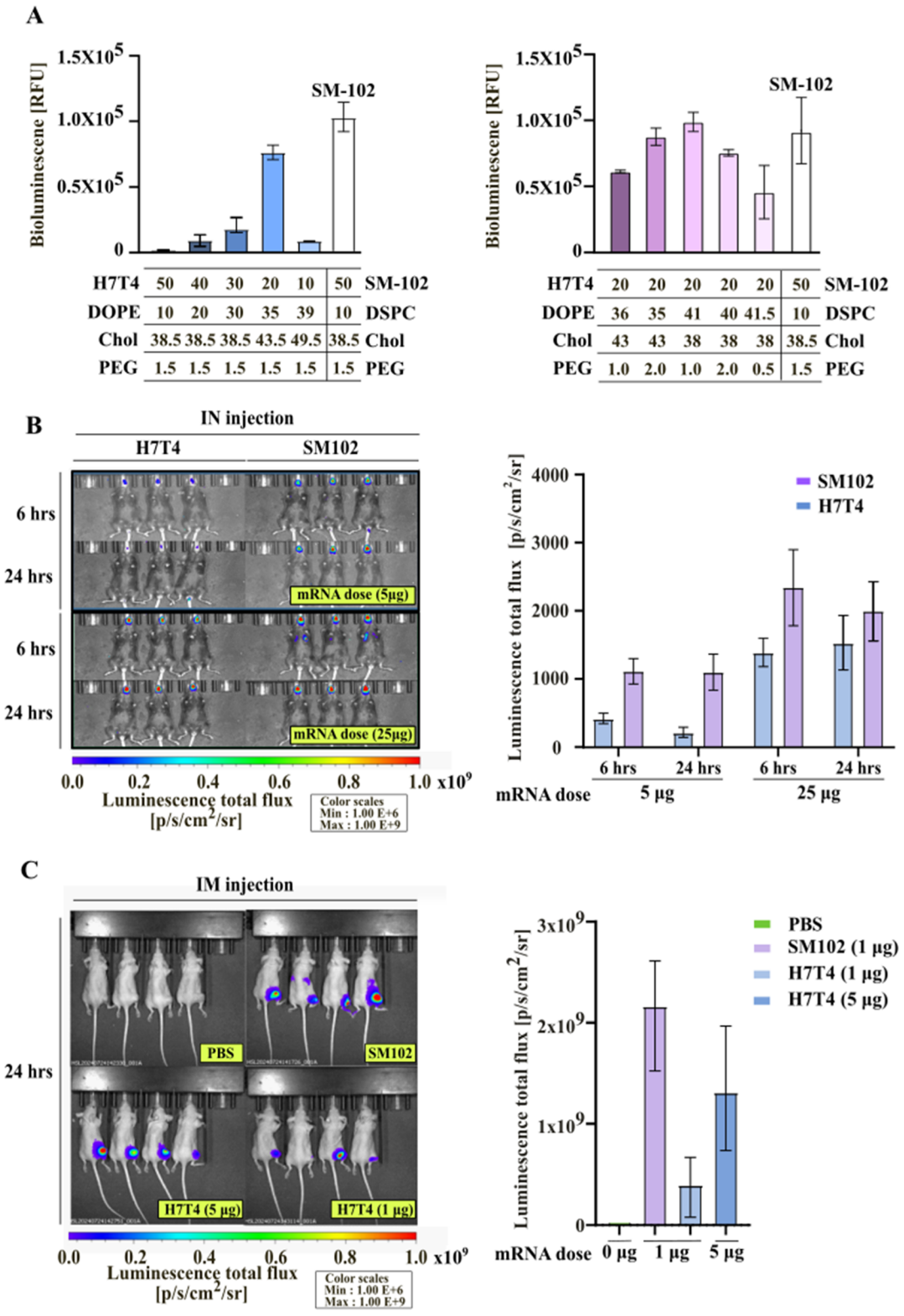

Figure 5. Optimization of H7T4−4 LNP formulation for mRNA delivery *in vitro* and *in vivo*. (A) *In vitro* firefly luciferase expression (n = 3, biologically independent samples). The pancreatic cancer cell line (AsPC-1) was treated with firefly luciferase mRNA-loaded H7T4 LNPs at a 10 ng/well mRNA dose for 24 h. (B) *In vivo* firefly luciferase expression (n = 4, biologically independent samples). Mice were injected intratumorally (i.t.) with firefly luciferase-loaded H7T4 LNPs at various mRNA doses (1 or 5 μg per mouse). IVIS luminescence imaging was performed at 24 h post-treatment, and total flux was quantified. (C) *In vivo* firefly luciferase expression (n = 3, biologically independent samples). Mice were administered intranasally (i.n.) with firefly luciferase-loaded H7T4 LNPs at various mRNA doses (5, 25 μg per mouse). IVIS luminescence imaging was performed at 6 and 24 h post-treatment, and total flux was quantified. Data are presented as mean ± SD. Statistical significance was evaluated using a one-way ANOVA with Tukey's post-hoc test for multiple comparisons.

https://doi.org/10.1021/acsami.5c06464
ACS Appl. Mater. Interfaces 2025, 17, 28012−28024

compared with SM-102 LNPs (50 mol %) represents a 2.5-fold reduction, offering potential cost advantages.

To evaluate the clinical potential, optimized H7T4 LNPs were tested for tumor-specific mRNA delivery. H7T4 LNPs encapsulating firefly luciferase mRNA were administered intratumorally to PANC1 pancreatic cancer xenografts at doses of 1 and 5 μg per mouse (Figure 5B). Luciferase expression was evaluated 24 h postinjection using an IVIS imaging system. Detection of luminescence signals in tumors at both dose levels confirmed the successful delivery of mRNA by all tested LNPs. H7T4 LNPs at 5 μg of mRNA dose showed comparable luciferase expression to SM102 LNPs containing 1 μg of mRNA. Although H7T4 LNPs showed lower overall transfection efficiency than SM-102 LNPs, they demonstrated superior tumor specificity, with higher mRNA accumulation and expression in tumor tissue relative to healthy tissues. In contrast, SM-102 LNPs showed substantial mRNA uptake in both the liver and spleen (Figure 5B).[66,67] This reduced off-target distribution enhances the therapeutic index of mRNA treatments by potentially minimizing immune-related adverse effects.

We next evaluated H7T4 LNPs for intranasal mRNA delivery by administering luciferase mRNA-loaded H7T4 LNPs intranasally at doses of 5 and 25 μg per mouse (Figure 5C). The IVIS imaging system was also used to quantify luminescence expression 6 and 24 h after injection. Despite achieving approximately 50% of the SM-102 LNP transfection efficiency, H7T4 LNPs demonstrated successful luciferase expression at both doses. Intranasal mRNA delivery represents a promising route for therapeutic applications, including vaccines, gene therapy, and treatments for respiratory and neurological conditions. This administration route offers key advantages: noninvasive delivery, avoidance of first-pass metabolism, and potential direct access to the lungs and brain via the olfactory pathway. These results suggest that H7T4 LNPs could serve as effective vehicles for intranasal mRNA delivery in clinical applications.

These results establish H7T4 LNPs as promising delivery vehicles for both tumor-targeted and intranasal mRNA therapeutics, offering the potential for diverse clinical applications.

CONCLUSIONS

Our study demonstrates that considering lipid transition temperature is crucial for rational LNP design. By selecting helper lipids with lower T_m to complement high-T_m ionizable lipids, such as H7T4−4, we successfully formulated stable mRNA/LNPs with enhanced mRNA delivery efficiency. This strategy provides a new framework for optimizing LNP components, potentially accelerating the development of effective mRNA therapeutics with improved specificity and reduced side effects. While our findings are promising, further research is needed to explore the generalizability of using T_m-guided helper lipid selection across different ionizable lipids. Additionally, investigating the long-term stability and immunogenicity of these LNP formulations will be crucial for clinical translation.

EXPERIMENTAL METHODS

Materials. Reagents and solvents were purchased from commercial vendors and used without further purification. SM-102 was purchased from BroadPharm (San Diego, CA, USA). Cholesterol, 1,2-distearoyl-*sn*-glycero-3-phosphorylcholine (DSPC), 1,2-dioleyl-*sn*-glycero-3-phospho-ethanolamine (DOPE), 1,2-di(9Z-octadecenoyl)-*sn*-glycero-3-phosphocholine (DOPC), 1,2-dioleoyl-*sn*-glycero-3-phospho-1′-rac-glycerol (DOPG), and 1,2-dimyristoyl-rac-glycero-3-methoxypolyethylene glycol-2000 (DMG-PEG 2000) were purchased from Avanti Polar Lipids (Birmingham, AL, USA). Pur-A-Lyzer dialysis cassette with 6 kDa MWCO (PURN60030), 50 kDa Amicon Ultra centrifugal filters (UFC9050). Cyclen tetrahydrochloride, 1,2-epoxytetradecane, and ethanol were purchased from Sigma-Aldrich (St. Louis, MO, USA). Quant-iT RiboGreen assay reagent (R11491) and TE buffer (20×) were purchased from Thermo Fischer Scientific (Waltham, MA, USA). Luciferase cell lysis buffer (5×) and luciferase assay reagent (E1501) were purchased from Promega (Madison, WI, USA).

Synthesis of the H7T4 Mixture. To a stirred solution of 1,4,7,10-tetraazacyclododecane (172 mg, 1.0 mmol, 1.0 equiv) and diisopropylethylamine (0.17 mL, 1.0 mmol, 1.0 equiv) in 4 mL of EtOH, 1,2-epoxytetradecane (212 mg, 1.0 mmol, 1.0 equiv) was added. The reaction mixture was then stirred for 24 h at room temperature, and the solvent was evaporated under reduced pressure. The mixture residues were purified by flash column chromatography (silica gel, CH_2Cl_2/MeOH, 70:30 v/v) to yield H7T4−1 (230 mg), H7T4−2 (16 mg), H7T4−3 (12 mg), and H7T4−4 (2.5 mg) as an amorphous solid.

Synthesis of H7T4−1. To a stirred solution of 1,4,7,10-tetraazacyclododecane (172 mg, 1.0 mmol, 1.0 equiv) and diisopropylethylamine (0.17 mL, 1.0 mmol, 1.0 equiv) in 4 mL of EtOH, 1,2-epoxytetradecane (212 mg, 1.0 mmol, 1.0 equiv) was added. The reaction mixture was then stirred for 24 h at room temperature, and the solvent was evaporated under reduced pressure. The residue was purified by flash column chromatography (silica gel, CH_2Cl_2/MeOH, 70:30 v/v) to yield H7T4−1 (230 mg, 60%) as an amorphous solid. ^{1}H NMR (400 MHz, $CDCl_3$): δ (ppm): 3.70−3.55 (2H, br s), 2.92−2.67 (12H, m), 2.67−2.54 (4H, m), 2.54−2.46 (1H, m), 2.41−2.29 (1H, m), 1.50−1.44 (2H, t, J = 7.2 Hz), 1.41−1.17(20H, m). 0.90(3H, t, J = 7.2 Hz). MALDI-TOF m/z: calcd for $C_{22}H_{48}N_4O$, 384.64; found, 385.96.

Synthesis of H7T4−2 and H7T4−3. To a stirred solution of 1,4,7,10-tetraazacyclododecane (172 mg, 1.0 mmol, 1.0 equiv) and diisopropylethylamine (0.54 mL, 3.0 mmol, 3.0 equiv) in 6 mL of EtOH, 1,2-epoxytetradecane (424 mg, 2.0 mmol, 2.0 equiv) was added. The reaction mixture was then stirred for 24 h at room temperature, and the solvent was evaporated under reduced pressure. The residue was purified by flash column chromatography (silica gel, CH_2Cl_2/MeOH, 80:20 v/v) to yield H7T4−2 (262 mg, 44%) and H7T4−3 (226 mg, 28%) as an amorphous solid, respectively. H7T4−2: ^{1}H NMR (400 MHz, $CDCl_3$): δ (ppm): 3.65 (2H, br s), 2.92−2.62 (14H, m), 2.62−2.52(4H, m), 2.43−2.40 (1H, m), 2.40−2.30 (1H, m), 1.49−1.14 (44H, m), 0.85 (6H, *t*, J = 7.2 Hz). MALDI-TOF m/z: calcd for $C_{36}H_{76}N_4O_2$, 597.01; found, 597.97. H7T3: ^{1}H NMR (400 MHz, $CDCl_3$): δ (ppm): MALDI-TOF m/z: calcd for $C_{50}H_{104}N_4O_3$, 809.39; found 809.99.

Synthesis of H7T4−4. To a stirred solution of 1,4,7,10-tetraazacyclododecane (172 mg, 1.0 mmol, 1.0 equiv) and diisopropylethylamine (1.0 mL, 6.0 mmol, 6.0 equiv) in 10 mL of EtOH, 1,2-epoxytetradecane (1.06 g, 5.0 mmol, 5.0 equiv) was added. The reaction mixture was then stirred for 24 h at room temperature, and the solvent was evaporated under reduced pressure. The residue was purified by flash column chromatography (silica gel, CH_2Cl_2/MeOH, 90:10 v/v) to yield H7T4−4 (664 mg, 65%) as a white solid. ^{1}H NMR (400 MHz, $CDCl_3$): δ (ppm): 5.05 (2H, s), 3.64 (4H, s), 2.97−2.64 (8H, m), 2.64−2.02 (16H, m), 1.52−1.14(88H, m), 0.85(12H, s). MALDI-TOF m/z: calcd for $C_{64}H_{132}N_4O_4$, 1021.76; found, 1022.75.

Messenger Ribonucleic Acid (mRNA). The mRNA for green fluorescence protein (GFP, CleanCap EGFP mRNA) and firefly luciferase (fLUP, CleanCap fLUC mRNA) were purchased from TriLink BioTechnologies, USA.

EGFP mRNA sequences were as follows. (AUGGUGAG-CAAGGGCGAGGAGCUGUUCACCGGGGUGGUGCCCAUC-CUGGUCGAGCUGGACGGCGACGUAAACGGCCACAAGUU-

https://doi.org/10.1021/acsami.5c06464
ACS Appl. Mater. Interfaces 2025, 17, 28012−28024

CAGCGUGUCCGGCGAGGGCGAGGGCGAUGCCAC-CUACGGCAAGCUGACCCUGAAGUUCAUCUGCACCACCGG-CAAGCUGCCCGUGCCCUGGCCCACCCUCGUGACCACCCU-GACCUACGGCGUGCAGUGCUUCAGCCGCUACCCCGACCA-CAUGAAGCAGCACGACUUCUUCAAGUCCGCCAUGCCC-GAAGGCUACGUCCAGGAGCGCACCAUCUUCUUCAAGGAC-GACGGCAACUACAAGACCCGCGCCGAGGUGAAGUUC-GAGGGCGACACCCUGGUGAACCGCAUCGAGCUGAAGGG-CAUCGACUUCAAGGAGGACGGCAACAUCCUGGGGCA-CAAGCUGGAGUACAACUACAACAGCCACAACGUCUAUAU-CAUGGCCGACAAGCAGAAGAACGGCAUCAAGGUGAACUU-CAAGAUCCGCCACAACAUCGAGGACGGCAGCGUGCAG-CUCGCCGACCACUACCAGCAGAACACCCCCAUCGGC-GACGGCCCCGUGCUGCUGCCCGACAACCACUACCUGAG-CACCCAGUCCGCCCUGAGCAAAGACCCCAACGA-GAAGCGCGAUCACAUGGUCCUGCUGGAGUUCGU-GACCGCCGCCGGGAUCACUCUCGGCAUGGACGAGCU-GUACAAGUAA).

FLUC mRNA sequences were as follows. (AUGGAGGACGC-CAAGAACAUCAAGAAGGGCCCCGCCCCCUUCUACCCC-CUGGAGGACGGCACCGCCGGCGAGCAGCUGCACAAGGC-CAUGAAGCGGUACGCCCUGGUGCCCGGCACCAUCGC-CUUCACCGACGCCCACAUCGAGGUGGACAUCAC-CUACGCCGAGUACUUCGAGAUGAGCGUGCGGCUGGCC-GAGGCCAUGAAGCGGUACGGCCUGAACACCAACCACCG-GAUCGUGGUGUGCAGCGAGAACAGCCUGCAGUUCUU-CAUGCCCGUGCUGGGCGCCCUGUUCAUCGGCGUGGCC-GUGGCCCCCGCCAACGACAUCUACAACGAGCGGGAGCUG-CUGAACAGCAUGGGCAUCAGCCAGCCCACCGUGGUGUUC-GUGAGCAAGAAGGGCCUGCAGAAGAUCCUGAACGUGCA-GAAGAAGCUGCCCAUCAUCCAGAAGAUCAUCAUCAUGGA-CAGCAAGACCGACUACCAGGGCUUCCAGAGCAUGUACAC-CUUCGUGACCAGCCACCUGCCCCCCGGCUUCAACGA-GUACGACUUCGUGCCCGAGAGCUUCGACCGGGACAAGAC-CAUCGCCCUGAUCAUGAACAGCAGCGGCAGCACCGGC-CUGCCCAAGGGCGUGGCCCUGCCCCACCGGACCGC-CUGCGUGCGGUUCAGCCACGCCCGGGACCCCAU-CUUCGGCAACCAGAUCAUCCCCGACACCGCCAUCCU-GAGCGUGGUGCCCUUCCACCACGGCUUCGGCAUGUU-CACCACCCUGGGCUACCUGAUCUGCGGCUUCCGGGUG-GUGCUGAUGUACCGGUUCGAGGAGGAGCUGUUCCUGCG-GAGCCUGCAGGACUACAAGAUCCAGAGCGCCCUGCUG-GUGCCCACCCUGUUCAGCUUCUUCGCCAAGAGCACCCU-GAUCGACAAGUACGACCUGAGCAACCUGCACGAGAUCGC-CAGCGGCGGCGCCCCCCUGAGCAAGGAGGUGGGC-GAGGCCGUGGCCAAGCGGUUCCACCUGCCCGG-CAUCCGGCAGGGCUACGGCCUGACCGAGACCACCAGCGC-CAUCCUGAUCACCCCCGAGGGCGACGA-CAAGCCCGGCGCCGUGGGCAAGGUGGUGCCCUUCUUC-GAGGCCAAGGUGGUGGACCUGGACACCGGCAAGACC-CUGGGCGUGAACCAGCGGGGCGAGCUGUGC-GUGCGGGGCCCCAUGAUCAUGAGCGGCUACGUGAA-CAACCCCGAGGCCACCAACGCCCUGAUCGACAAGGACGG-CUGGCUGCACAGCGGCGACAUCGCCUACUGGGACGAG-GACGAGCACUUCUUCAUCGUGGACCGGCUGAAGAGCCU-GAUCAAGUACAAGGGCUACCAGGUGGCCCCCGCCGAG-CUGGAGAGCAUCCUGCUGCAGCACCCCAACAUCUUC-GACGCCGGCGUGGCCGGCCUGCCCGACGAC-GACGCCGGCGAGCUGCCCGCCGCCGUGGUGGUGCUG-GAGCACGGCAAGACCAUGACCGAGAAGGAGAUCGUGGA-CUACGUGGCCAGCCAGGUGACCACCGCCAAGAAG-CUGCGGGGCGGCGUGGUGUUCGUGGACGAGGUGCC-CAAGGGCCUGACCGGCAAGCUGGACGCCCGGAA-GAUCCGGGAGAUCCUGAUCAAGGCCAAGAAGGGCGGCAA-GAUCGCCGUGUGA). The mRNA was prepared using CleanCap technology as per the manufacturer's instructions. The stock mRNA sequences were provided as such without further modifications.

Lipid Nanoparticle (LNP) Formulation. The LNPs were prepared by pipet mixing or Nano Assemblr Ignite (Vancouver, Canada). Lipid components (SM-102:cholesterol/DSPC:DMG-PEG 2000 50:39.5:10:1.5 or H7T4:cholesterol/DOPE:DMG-PEG 2000 with various molar ratios) and mRNA were dissolved in ethanol and 50 mM citrate buffer (pH 4.0), respectively, with a 1:3 volume ratio. The weight ratio (w/w = 10) of the ionizable lipid to mRNA was used. For pipet mixing, the buffer solution containing mRNA was added to the lipid components solution, and the mixture was vigorously mixed by pipet and vortexed. For the nanoassembly of ignite, two prepared solutions were uniformly mixed at a 12 mL/min flow rate. Then, the formulated LNP solution was incubated at room temperature for 30 min and dialyzed against PBS buffer by using a Pur-A-Lyzer dialysis cassette with 6 kDa MWCO overnight. The LNP was concentrated using 50 kDa Amicon Ultra centrifugal filters at 4000 rpm for 30 min, stored at 4 °C for up to 1 week before use, and used for further characterization and transfection.

Optimization of mRNA/LNP Formulation. The design of the experiment (DoE) and fractional factorial design strategy were adopted to optimize the mRNA/LNP formulation conditions. At the first screening, the DoE strategy with 1 four-level qualitative factor (helper lipid type) and 3 four-level quantitative factors (ionizable lipid %, PEG lipid %, helper lipid %) was employed to determine the significant factors. At the second screening, 33 fractional factorial designed strategies with 1 three-level qualitative factor (helper lipid type) were used to maximize the delivery performance of LNP.

Characterization of the Size, Zeta Potential, and Encapsulation Efficiency of mRNA/LNPs. For the LNP size and polydispersity index, the LNP stock solution was diluted in pH 7.4 PBS buffer at a 1:100 ratio, and the diluted LNP solution was equilibrated at room temperature. The size distribution was measured in triplicate using dynamic light scattering performed on a Malvern Zetasizer Nano (Malvern, UK). The mRNA concentration and encapsulation efficacy of LNPs were determined by using a Quant-iT RiboGreen assay. The LNP stock solution was diluted in RNase-free distilled TE buffer or 2% Triton-X-containing TE buffer in a 1:200 ratio. The corresponding mRNA was prepared in TE buffer and 2% Triton-X-containing TE buffer by a serial dilution (1 to 0.0625 μL/mL) for a standard curve. The LNP and mRNA solution (100 μL) was transferred to a black 96-well plate, and the assay was performed in triplicate. The RiboGreen reagent solution was prepared in TE buffer by a 1:200 dilution and then added to each well (100 μL). The fluorescence intensity was measured with a Tecan Infinite plate reader (excitation 485 nm/emission 525 nm). The fluorescence intensity was corrected by subtracting the background fluorescence. The corrected fluorescence intensity was converted to mRNA concentration, as followed by the standard curve, and the encapsulated mRNA concentration was determined by subtracting an exterior mRNA concentration from a total mRNA concentration. The encapsulation efficacy was calculated from the ratio of the interior mRNA concentration to the total mRNA concentration.

Cryogenic Transmission Electron Microscopy (Cryo-TEM) of mRNA/LNPs. The EM grids were glow-discharged for 60 s at 15 mA before sample application. 3 μL of LNPs were applied to Quantifoil holey carbon EM grids (R1.2/1.3, 200 mesh; EMS) and blotted with Vitrobot Mark IV (FEI) using 3s blotting time with 100% relative humidity at 4 °C. Samples were imaged on Glacios (FEI) at an acceleration voltage of 200 kV with a Falcon IV direct electron detector (FEI). Images were taken at 97,000× magnification and defocus −3.0 μm.

Small-Angle X-Ray Scattering (SAXS) Analysis of mRNA/LNPs. SAXS experiments were conducted using a BioXolver from Xenocs, provided by the Korea Basic Science Institute (KBSI). The setup featured a Dectris EIGER2 Si 1 M detector and utilized a Gallium MetalJet X-ray source (Ga D2+) operated at 70 kV, generating X-rays with a wavelength of 1.34144×10^{-10} m. Measurements were carried out using 12 μL of sample volume in a 2 mm quartz capillary. The experiments were performed in the SAXS2 mode with a sample-to-detector distance of 900 mm, covering a q-range from 0.01 to 0.34 $Å^{-1}$.

Each measurement involved an exposure time of 360 s, collected over 10 frames per sample. The resulting scattering patterns were averaged to enhance the signal-to-noise ratio. The scattering pattern

https://doi.org/10.1021/acsami.5c06464
ACS Appl. Mater. Interfaces 2025, 17, 28012−28024

of the buffer was subtracted from the averaged sample data to obtain the differential scattering profile. Data analysis included averaging the frames and verifying the subtracted data to ensure reliability through standard data reduction and normalization procedures.

Nano Differential Scanning Calorimetry (nDSC) Analysis of mRNA/LNPs. Nano differential scanning calorimetry (nDSC) measurements were obtained by TA Instruments (New Castle, DE) nano DSC-6300. Samples were scanned at heating/cooling rates of 1 °C/min, using 1−2 mg of lipid. Samples were run 5−15 min after preparation unless otherwise noted, and the first heating scans were reported. However, the first and second heating scans were identical for mRNA/LNPs.

Cell Culture. The human embryonic kidney HEK293T (CRL-3216), mouse myoblast cell line C2C12 (CRL-1772), and human pancreatic cancer cell line AsPC-1 (CRL-1682) were incubated under standard conditions (5% CO2, 37 °C). HEK293T cells were cultured in RPMI-1640 with L-glutamine (Welgene) supplemented with 10% FBS and 2% 1 mM mercaptoethanol. C2C12 cells and AsPC-1 cells were cultured in DMEM with L-glutamine (Welgene) supplemented with 10% FBS.

***In Vitro* Transfection.** HEK293T cells were cultured in RPMI1640 with L-glutamine supplemented with 10% FBS and 2% mercaptoethanol. AsPC-1 cells and C2C12 cells were cultured in DMEM with L-glutamine supplemented with 10% FBS. AsPC-1 cells and C2C12 cells (5×10^3 per well) were plated in a white 96-well plate, and HEK293T cells (5×10^3 per well) were plated in a transparent 6-well plate in triplicate in media (1 mL) and incubated at 37 °C for 24 h. In the case of *in vitro* transfection, Lipofectamine MessengermMAX (Thermo Fisher Scientific) was used following the manufacturer's protocol. 5 μL/well of opti-MEM (Thermo Fisher Scientific) was mixed with 0.225 μL/well of Lipofectamine MessengerMAX, and 5 μL/well of opti-MEM was mixed with mRNAs. The mRNA mixture was added into each well and incubated at 37 °C. The mRNA mixture-containing medium was removed from the well and washed with PBS buffer (×2). Then, each well was treated with cell lysis reagent and left at room temperature for 3 min. Each well was treated with the Nano-Glo Luciferase Assay System (Promega) for NlucP and the Luciferase Assay System (Promega) for Fluc, and the relative luminescence intensity was measured with a Tecan Infinite plate reader.

Evaluation of *In Vitro* Fluorescence. HEK293T cells were cultured in RPMI1640 with L-glutamine supplemented with 10% FBS and 2% mercaptoethanol. HEK293T (5×10^3 per well) was plated in a transparent 6-well plate in triplicate in media (1 mL) and incubated at 37 °C for 24 h. The LNP solution was diluted in PBS buffer as a 5 ng/μL mRNA dose. The LNP solution was added to each well and incubated at 37 °C for 24 h. Fluorescent microscopy was used to detect the expression of GFP. The GFP fluorescence was imaged under a fluorescence microscope equipped with a multichannel laser system for detecting the green wavelength (488 nm) (IX83, Olympus, USA). The fluorescent images were processed and merged with the brightfield images using ImageJ (v1.54 g, ImageJ, NIH, USA).

Evaluation of *In Vitro* Luminescence. AsPC-1 cells and C2C12 cells were cultured in DMEM with L-glutamine supplemented with 10% FBS. AsPC-1 cells and C2C12 cells (5×10^3 per well) were plated in a white 96-well plate in triplicate in media (100 μL) and incubated at 37 °C for 24 h. The LNP solution was diluted in PBS buffer as a 5 ng/μL mRNA dose. The LNP solution was added into each well and incubated at 37 °C for 24 h. The LNP solution containing media was removed from the well and washed with PBS buffer (×2). Then, each well was treated with cell lysis reagent and left at room temperature for 3 min. Each well was treated with firefly luciferase reagent (Promega), and the relative luminescence intensity was measured with a Tecan Infinite plate reader.

Tumor Xenograft Study. All animal experiments were carried out under the guidelines of the Korea Research Institute of Bioscience & Biotechnology (KRIBB)'s Institutional Animal Care and Use Committee (IACUC approval number: KRIBB-AEC-24163). For the mouse xenograft model, PANC1 cells (1×10^7 cells in 50% matrigel) were subcutaneously injected into the right thigh of female 5 week-old BALB/c nude mice. The experiments were conducted when the tumor size reached 200 mm^3. Tumor volume was calculated using the following formula: V (mm^3) = $0.5 \times L \times W2$ (V: volume, L: length, and W: width). Mice were monitored regularly every 3−4 days, administered intratumorally with each LNP sample, and euthanized at the indicated time points for IVIS imaging and organ harvest.

Evaluation of *In Vivo* Bioluminescence. All animal studies were approved by the Institutional Animal Care and Use Committee (IACUC) of the Korea Research Institute of Bioscience and Biotechnology (KRIBB). Female C57BL/6 mice (Orient Bio, 5−6 weeks age, 18−22 g) were intramuscularly or intranasally injected at one side of a thigh with LNPs containing firefly luciferase mRNA (1 and 5 μg for the intramuscular route or 5 and 25 μg for the intranasal route, 50 μL for the intramuscular route and 30 μL for the intranasal route). The mice were anesthetized using isoflurane at 6 or 24 h after administration. D-luciferin (3 mg, 200 μL) was administered to mice via intraperitoneal injection. Then, after 15 min, the bioluminescence was recorded using an IVIS imaging system (PerkinElmer, Waltham, MA) and quantified using LivingImage software (PerkinElmer) to measure the radiance in photons/sec.

■ ASSOCIATED CONTENT

Supporting Information

The Supporting Information is available free of charge at https://pubs.acs.org/doi/10.1021/acsami.5c06464.

Information on materials and methods includes LNP composition, cryo-TEM, SAXS, nDSC fluorescence imaging, and bioluminescence analysis (PDF)

■ AUTHOR INFORMATION

Corresponding Authors

Jeong Kyu Bang − *Division of Magnetic Resonance, Korea Basic Science Institute (KBSI), Ochang 28116, Republic of Korea; Dandicure Inc, Ochang, Chung Buk 28119, Republic of Korea;* orcid.org/0000-0001-5916-0912; Email: bangjk@kbsi.re.kr

Michael J. Mitchell − *Department of Bioengineering, University of Pennsylvania, Philadelphia, Pennsylvania 19104, United States;* orcid.org/0000-0002-3628-2244; Email: mjmitch@seas.upenn.edu

Hyunjoo Cha-Molstad − *Nucleic Acid Therapeutics Research Center, Korea Research Institute of Bioscience and Biotechnology (KRIBB), Ochang 28116, Republic of Korea; Advanced Bioconvergence Department, KRIBB School, University of Science and Technology, Deajeon 34113, Republic of Korea;* orcid.org/0000-0003-3676-7150; Email: hcha@kribb.re.kr

Authors

Jeong Eun Shin − *Nucleic Acid Therapeutics Research Center, Korea Research Institute of Bioscience and Biotechnology (KRIBB), Ochang 28116, Republic of Korea;* orcid.org/0000-0002-5986-7069

Eun-jeong Won − *Nucleic Acid Therapeutics Research Center, Korea Research Institute of Bioscience and Biotechnology (KRIBB), Ochang 28116, Republic of Korea;* orcid.org/0000-0003-4517-3434

Junchao Xu − *Department of Bioengineering, University of Pennsylvania, Philadelphia, Pennsylvania 19104, United States;* orcid.org/0000-0003-0725-8111

Jong Cheol Lee − *Dandicure Inc, Ochang, Chung Buk 28119, Republic of Korea;* orcid.org/0009-0002-5779-0763

Complete contact information is available at: https://pubs.acs.org/10.1021/acsami.5c06464

Author Contributions

[#]J.K.B., M.J.M., and H.C.-M. contributed equally to this work.Design and synthesis of ionizable lipids and the design of experiments (DoE) of LNPs were performed by J.E.S., J.X., and J.K.B. Synthesis and structural analysis of target ionizable lipids were conducted by J.-C.L. Analysis of *in vitro* and luminescence was performed by J.E.S. Analysis of the tumor xenograft model was performed by E.J.W. H.C.-M., M.J.M., and J.K.B. conceptualized the study and designed the experiments. All first and corresponding authors were involved in writing the paper.

Funding

This research was supported by the National Research Council of Science & Technology (NST) grant (No. GTL24021-000), the Nano & Material Technology Development Program through the National Research Foundation of Korea (NRF) (RS-2024-00444177), the Korea Research Institute of Bioscience and Biotechnology (KRIBB) Research Initiative Program (KGM1062413), and the grant (C539200) from Korea Basic Science Institute (KBSI), all funded by the Korea government (MSIT).

Notes

The authors declare no competing financial interest.

■ ACKNOWLEDGMENTS

We thank Professor Sangyong Jon and Dr. Sunyoung Kim at the Korea Advanced Institute of Science and Technology (KAIST) for assistance with IVIS, Joonhyeok Choi at the Korea Basic Science Institute (KBSI, Ochang, Korea) for assistance with SAXS experiments, and the Imaging Analysis Team at the Korea Research Institute of Bioscience and Biotechnology (KRIBB) for assistance with cryo-TEM.

■ ABBREVIATIONS

DoE, design of experiment; DOPC, 1,2-di(9*Z*-octadecenoyl)-*sn*-glycero-3-phosphocholine; DOPE, 1,2-dioleoyl-*sn*-glycero-3-phosphoethanolamine; DOPG, 1,2-dioleoyl-*sn*-glycero-3-phosphoglycerol; DSPC, 1,2-distearoyl-*sn*-glycero-3-phosphocholine; LNP, lipid nanoparticle; nDSC, nano differential scanning calorimetry; SAXS, small-angle X-ray scattering; Cryo-TEM, cryogenic transmission electron microscope; FBS, fetal bovine serum; Fluc, firefly luciferase; i.m., intramuscular; i.n., intranasal; IACUC, Institutional Animal Care and Use Committee; KRIBB, Korea Research Institute of Bioscience and Biotechnology.

■ REFERENCES

(1) Li, J.; Zhang, Y.; Yang, Y. G.; Sun, T. Advancing mRNA Therapeutics: The Role and Future of Nanoparticle Delivery Systems. *Mol. Pharmaceutics* **2024**, *21* (8), 3743−3763.

(2) Qin, S.; Tang, X.; Chen, Y.; Chen, K.; Fan, N.; Xiao, W.; Zheng, Q.; Li, G.; Teng, Y.; Wu, M.; et al. mRNA-based therapeutics: powerful and versatile tools to combat diseases. *Signal Transduction Targeted Ther.* **2022**, *7* (1), 166.

(3) Hussain, M. S.; Khan, G. Current clinical applications of RNA-LNPs in cancer: a promising horizon for targeted therapies. *EXCLI Journal* **2025**, *24*, 321−324.

(4) Wang, B.; Shen, B.; Xiang, W.; Shen, H. Advances in the study of LNPs for mRNA delivery and clinical applications. *Virus Genes* **2024**, *60* (6), 577−591.

(5) Sarnelli, S.; Cardamone, M.; Reverchon, E.; Baldino, L. Lipid-Based Nanoparticles for Nucleic Acids Delivery. *Phys. Sci. Rev.* **2025**, *10*, 317−338.

(6) De, A.; Ko, Y. A. Tale of Nucleic Acid−Ionizable Lipid Nanoparticles: Design and Manufacturing Technology and Advancement. *Expert Opin. Drug Deliver* **2023**, *20* (1), 75−91.

(7) Swetha, K.; Kotla, N. G.; Tunki, L.; Jayaraj, A.; Bhargava, S. K.; Hu, H.; Bonam, S. R.; Kurapati, R. Recent Advances in the Lipid Nanoparticle-Mediated Delivery of mRNA Vaccines. *Vaccines* **2023**, *11* (3), 658.

(8) Hagedorn, L.; Jurgens, D. C.; Merkel, O. M.; Winkeljann, B. Endosomal escape mechanisms of extracellular vesicle-based drug carriers: lessons for lipid nanoparticle design. *Extracell. Vesicles Circ. Nucleic Acids* **2024**, *5* (3), 344−357.

(9) Xu, Y.; Golubovic, A.; Xu, S.; Pan, A.; Li, B. Rational design and combinatorial chemistry of ionizable lipids for RNA delivery. *J. Mater. Chem. B* **2023**, *11* (28), 6527−6539.

(10) Petersen, D. M. S.; Weiss, R. M.; Hajj, K. A.; Yerneni, S. S.; Chaudhary, N.; Newby, A. N.; Arral, M. L.; Whitehead, K. A. Branched-Tail Lipid Nanoparticles for Intravenous mRNA Delivery to Lung Immune, Endothelial, and Alveolar Cells in Mice. *Adv. Healthcare Mater.* **2024**, *13* (22), No. e2400225.

(11) Sun, D.; Lu, Z. R. Structure and Function of Cationic and Ionizable Lipids for Nucleic Acid Delivery. *Pharm. Res.* **2023**, *40* (1), 27−46.

(12) Han, X.; Zhang, H.; Butowska, K.; Swingle, K. L.; Alameh, M. G.; Weissman, D.; Mitchell, M. J. An ionizable lipid toolbox for RNA delivery. *Nat. Commun.* **2021**, *12* (1), 7233.

(13) Herrera, M.; Kim, J.; Eygeris, Y.; Jozic, A.; Sahay, G. Illuminating endosomal escape of polymorphic lipid nanoparticles that boost mRNA delivery. *Biomater. Sci.* **2021**, *9* (12), 4289−4300.

(14) Hou, X.; Zaks, T.; Langer, R.; Dong, Y. Lipid nanoparticles for mRNA delivery. *Nat. Rev. Mater.* **2021**, *6* (12), 1078−1094.

(15) Philipp, J.; Dabkowska, A.; Reiser, A.; Frank, K.; Krzyszton, R.; Brummer, C.; Nickel, B.; Blanchet, C. E.; Sudarsan, A.; Ibrahim, M.; et al. pH-dependent structural transitions in cationic ionizable lipid mesophases are critical for lipid nanoparticle function. *Proc. Natl. Acad. Sci. U.S.A.* **2023**, *120* (50), No. e2310491120.

(16) Tesei, G.; Hsiao, Y. W.; Dabkowska, A.; Gronberg, G.; Yanez Arteta, M.; Ulkoski, D.; Bray, D. J.; Trulsson, M.; Ulander, J.; Lund, M.; et al. Lipid shape and packing are key for optimal design of pH-sensitive mRNA lipid nanoparticles. *Proc. Natl. Acad. Sci. U.S.A.* **2024**, *121* (2), No. e2311700120.

(17) Budai, L.; Budai, M.; Bozo, T.; Agocs, G.; Kellermayer, M.; Antal, I. Determination of the Main Phase Transition Temperature of Phospholipids by Oscillatory Rheology. *Molecules* **2023**, *28* (13), 5125.

(18) Albon, N.; Sturtevant, J. M. Nature of the gel to liquid crystal transition of synthetic phosphatidylcholines. *Proc. Natl. Acad. Sci. U.S.A.* **1978**, *75* (5), 2258−2260.

(19) Leekumjorn, S.; Sum, A. K. Molecular characterization of gel and liquid-crystalline structures of fully hydrated POPC and POPE bilayers. *J. Phys. Chem. B* **2007**, *111* (21), 6026−6033.

(20) Valldeperas, M.; Dabkowska, A. P.; Palsson, G. K.; Rogers, S.; Mahmoudi, N.; Carnerup, A.; Barauskas, J.; Nylander, T. Interfacial properties of lipid sponge-like nanoparticles and the role of stabilizer on particle structure and surface interactions. *Soft Matter* **2019**, *15* (10), 2178−2189.

(21) Roux, M.; Bonnet, V.; Djedaini-Pilard, F. Ordering of Saturated and Unsaturated Lipid Membranes near Their Phase Transitions Induced by an Amphiphilic Cyclodextrin and Cholesterol. *Langmuir* **2019**, *35* (44), 14376−14387.

(22) Blok, M. C.; van der Neut-Kok, E. C.; van Deenen, L. L.; de Gier, J. The effect of chain length and lipid phase transitions on the selective permeability properties of liposomes. *Biochim. Biophys. Acta* **1975**, *406* (2), 187−196.

(23) Cevc, G. How membrane chain-melting phase-transition temperature is affected by the lipid chain asymmetry and degree of unsaturation: an effective chain-length model. *Biochemistry* **1991**, *30* (29), 7186−7193.

https://doi.org/10.1021/acsami.5c06464
ACS Appl. Mater. Interfaces 2025, 17, 28012−28024

(24) Marsh, D. Structural and thermodynamic determinants of chain-melting transition temperatures for phospholipid and glycolipids membranes. *Biochim. Biophys. Acta* **2010**, *1798* (1), 40−51.
(25) Briuglia, M. L.; Rotella, C.; McFarlane, A.; Lamprou, D. A. Influence of cholesterol on liposome stability and on in vitro drug release. *Drug Delivery Transl. Res.* **2015**, *5* (3), 231−242.
(26) Ortega, D. D.; Pavlakovich, N.; Shon, Y. S. Effects of lipid bilayer encapsulation and lipid composition on the catalytic activity and colloidal stability of hydrophobic palladium nanoparticles in water. *RSC Adv.* **2022**, *12* (34), 21866−21874.
(27) Bak, A.; Zhou, L.; Rejman, J.; Yanez Arteta, M.; Nilsson, G.; Ashford, M. Roadmap to Discovery and Early Development of an mRNA-Loaded LNP Formulation for Liver Therapeutic Genome Editing. *Expert Opin. Drug Delivery* **2025**, *22* (2), 239−254.
(28) Cui, L.; Pereira, S.; Sonzini, S.; van Pelt, S.; Romanelli, S.; Liang, L.; Ulkoski, D.; Krishnamurthy, V. R.; Brannigan, E.; Brankin, C.; et al. Development of a High-Throughput Platform for Screening Lipid Nanoparticles for mRNA Delivery. *Nanoscale* **2022**, *14*, 1480−1491.
(29) Pratsinis, A.; Fan, Y.; Portmann, M.; Hammel, M.; Kou, P.; Sarode, A.; Ringler, P.; Kovacik, L.; Lauer, M. E.; Lamerz, J.; et al. Impact of Non-Ionizable Lipids and Phase Mixing Methods on Structural Properties of Lipid Nanoparticle Formulations. *Int. J. Pharm.* **2023**, *637*, 122874.
(30) Gurba-Bryśkiewicz, L.; Maruszak, W.; Smuga, D.; Dubiel, K.; Wieczorek, M. Quality by Design (QbD) and Design of Experiments (DOE) as a Strategy for Tuning Lipid Nanoparticle Formulations for RNA Delivery. *Biomedicines* **2023**, *11* (10), 2752.
(31) Hashiba, K.; Taguchi, M.; Sakamoto, S.; Otsu, A.; Maeda, Y.; Ebe, H.; Okazaki, A.; Harashima, H.; Sato, Y. Overcoming Thermostability Challenges in mRNA−Lipid Nanoparticle Systems with Piperidine-Based Ionizable Lipids. *Commun. Biol.* **2024**, *7*, 556.
(32) Mehta, M.; Bui, T.; Yang, X.; Aksoy, Y.; Goldys, E.; Deng, W. Lipid-Based Nanoparticles for Drug/Gene Delivery: An Overview of the Production Techniques and Difficulties Encountered in Their Industrial Development. *ACS Mater. Au* **2023**, *3* (6), 600−619.
(33) Rampado, R.; Peer, D. Design of Experiments in the Optimization of Nanoparticle-Based Drug Delivery Systems. *J. Controlled Release* **2023**, *358*, 398−419.
(34) Barbieri, B.; Peeler, D.; Samnuan, K.; Day, S.; Hu, K.; Sallah, H. J.; Tregoning, J. S.; McKay, P. F.; Shattock, R. J. The role of helper lipids in optimising nanoparticle formulations of self-amplifying RNA. *J. Controlled Release* **2024**, *374*, 280−292.
(35) Cullis, P.; Felgner, P. The 60-Year Evolution of Lipid Nanoparticles for Nucleic Acid Delivery. *Nat. Rev. Drug Discovery* **2024**, *23* (9), 709−722.
(36) Jia, Y.; Wang, X.; Li, L.; Li, F.; Zhang, J.; Liang, X. Lipid Nanoparticles Optimized for Targeting and Release of Nucleic Acid. *Adv. Mater.* **2024**, *36* (4), No. e2305300.
(37) LoPresti, S.; Arral, M.; Chaudhary, N.; Whitehead, K. A. The Replacement of Helper Lipids with Charged Alternatives in Lipid Nanoparticles Facilitates Targeted mRNA Delivery to the Spleen and Lungs. *J. Controlled Release* **2022**, *345*, 819−831.
(38) Tang, X.; Zhang, Y.; Han, X. Ionizable Lipid Nanoparticles for mRNA Delivery. *Adv. NanoBiomed Res.* **2023**, *3*, 2300006.
(39) Mendonca, M. C. P.; Kont, A.; Kowalski, P. S.; O'Driscoll, C. M. Design of lipid-based nanoparticles for delivery of therapeutic nucleic acids. *Drug Discovery Today* **2023**, *28* (3), 103505.
(40) Zeng, Y.; Escalona-Rayo, O.; Knol, R.; Kros, A.; Slutter, B. Lipid nanoparticle-based mRNA candidates elicit potent T cell responses. *Biomater. Sci.* **2023**, *11* (3), 964−974.
(41) Barbieri, B. D.; Peeler, D. J.; Samnuan, K.; Day, S.; Hu, K.; Sallah, H. J.; Tregoning, J. S.; McKay, P. F.; Shattock, R. J. The role of helper lipids in optimizing nanoparticle formulations of self-amplifying RNA. *J. Controlled Release* **2024**, *374*, 280−292.
(42) Cheng, X.; Lee, R. J. The role of helper lipids in lipid nanoparticles (LNPs) designed for oligonucleotide delivery. *Adv. Drug Deliv Rev.* **2016**, *99* (Pt A), 129−137.
(43) Hui, S. W.; Langner, M.; Zhao, Y. L.; Ross, P.; Hurley, E.; Chan, K. The role of helper lipids in cationic liposome-mediated gene transfer. *Biophys. J.* **1996**, *71* (2), 590−599.
(44) Chen, W.; Dusa, F.; Witos, J.; Ruokonen, S. K.; Wiedmer, S. K. Determination of the Main Phase Transition Temperature of Phospholipids by Nanoplasmonic Sensing. *Sci. Rep.* **2018**, *8* (1), 14815.
(45) Markova, N.; Cairns, S.; Jankevics-Jones, H.; Kaszuba, M.; Caputo, F.; Parot, J. Biophysical Characterization of Viral and Lipid-Based Vectors for Vaccines and Therapeutics with Light Scattering and Calorimetric Techniques. *Vaccines* **2022**, *10* (1), 49.
(46) Bolean, M.; Simao, A. M.; Favarin, B. Z.; Millan, J. L.; Ciancaglini, P. The effect of cholesterol on the reconstitution of alkaline phosphatase into liposomes. *Biophys. Chem.* **2010**, *152* (1−3), 74−79.
(47) Drazenovic, J.; Wang, H.; Roth, K.; Zhang, J.; Ahmed, S.; Chen, Y.; Bothun, G.; Wunder, S. L. Effect of lamellarity and size on calorimetric phase transitions in single component phosphatidylcholine vesicles. *Biochim. Biophys. Acta* **2015**, *1848* (2), 532−543.
(48) McMullen, T. P.; Lewis, R. N.; McElhaney, R. N. Differential scanning calorimetric study of the effect of cholesterol on the thermotropic phase behavior of a homologous series of linear saturated phosphatidylcholines. *Biochemistry* **1993**, *32* (2), 516−522.
(49) Chen, L.; Johnson, M. L.; Biltonen, R. L. A macroscopic description of lipid bilayer phase transitions of mixed-chain phosphatidylcholines: chain-length and chain-asymmetry dependence. *Biophys. J.* **2001**, *80* (1), 254−270.
(50) Matsuki, H.; Miyazaki, E.; Sakano, F.; Tamai, N.; Kaneshina, S. Thermotropic and barotropic phase transitions in bilayer membranes of ether-linked phospholipids with varying alkyl chain lengths. *Biochim. Biophys. Acta, Biomembr.* **2007**, *1768* (3), 479−489.
(51) Fedorovskiy, A. G.; Antropov, D. N.; Dome, A. S.; Puchkov, P. A.; Makarova, D. M.; Konopleva, M. V.; Matveeva, A. M.; Panova, E. A.; Shmendel, E. V.; Maslov, M. A.; et al. Novel Efficient Lipid-Based Delivery Systems Enable a Delayed Uptake and Sustained Expression of mRNA in Human Cells and Mouse Tissues. *Pharmaceutics* **2024**, *16* (5), 684.
(52) Yu, H.; Iscaro, J.; Dyett, B.; Zhang, Y.; Seibt, S.; Martinez, N.; White, J.; Drummond, C. J.; Bozinovski, S.; Zhai, J. Inverse Cubic and Hexagonal Mesophase Evolution within Ionizable Lipid Nanoparticles Correlates with mRNA Transfection in Macrophages. *J. Am. Chem. Soc.* **2023**, 24765−24774.
(53) Pattipeiluhu, R.; Zeng, Y.; Hendrix, M.; Voets, I. K.; Kros, A.; Sharp, T. H. Liquid crystalline inverted lipid phases encapsulating siRNA enhance lipid nanoparticle mediated transfection. *Nat. Commun.* **2024**, *15* (1), 1303.
(54) Zheng, L.; Bandara, S. R.; Tan, Z.; Leal, C. Lipid nanoparticle topology regulates endosomal escape and delivery of RNA to the cytoplasm. *Proc. Natl. Acad. Sci. U.S.A.* **2023**, *120* (27), No. e2301067120.
(55) Gujrati, M.; Malamas, A.; Shin, T.; Jin, E.; Sun, Y.; Lu, Z. R. Multifunctional cationic lipid-based nanoparticles facilitate endosomal escape and reduction-triggered cytosolic siRNA release. *Mol. Pharmaceutics* **2014**, *11* (8), 2734−2744.
(56) Askarizadeh, A.; Vahdat-Lasemi, F.; Karav, S.; Kesharwani, P.; Sahebkar, A. Lipid nanoparticle-based delivery of small interfering RNAs: New possibilities in the treatment of diverse diseases. *Eur. Polym. J.* **2025**, *223*, 113624.
(57) Li, S.; Hu, Y.; Li, A.; Lin, J.; Hsieh, K.; Schneiderman, Z.; Zhang, P.; Zhu, Y.; Qiu, C.; Kokkoli, E.; et al. Payload distribution and capacity of mRNA lipid nanoparticles. *Nat. Commun.* **2022**, *13* (1), 5561.
(58) Brader, M. L.; Williams, S. J.; Banks, J. M.; Hui, W. H.; Zhou, Z. H.; Jin, L. Encapsulation state of messenger RNA inside lipid nanoparticles. *Biophys. J.* **2021**, *120* (14), 2766−2770.
(59) Boggs, J. M. Effect of lipid structural modifications on their intermolecular hydrogen bonding interactions and membrane functions. *Biochem. Cell Biol.* **1986**, *64* (1), 50−57.

https://doi.org/10.1021/acsami.5c06464
ACS Appl. Mater. Interfaces 2025, 17, 28012−28024

(60) Schonfeldova, T.; Piller, P.; Kovacik, F.; Pabst, G.; Okur, H. I.; Roke, S. Lipid Melting Transitions Involve Structural Redistribution of Interfacial Water. *J. Phys. Chem. B* **2021**, *125* (45), 12457−12465.
(61) Kolasinac, R.; Kleusch, C.; Braun, T.; Merkel, R.; Csiszar, A. Deciphering the Functional Composition of Fusogenic Liposomes. *Int. J. Mol. Sci.* **2018**, *19* (2), 346.
(62) Yaghmur, A.; Laggner, P.; Zhang, S.; Rappolt, M. Tuning curvature and stability of monoolein bilayers by designer lipid-like peptide surfactants. *PLoS One* **2007**, *2* (5), No. e479.
(63) Graewert, M. A.; Wilhelmy, C.; Bacic, T.; Schumacher, J.; Blanchet, C.; Meier, F.; Drexel, R.; Welz, R.; Kolb, B.; Bartels, K.; et al. Quantitative size-resolved characterization of mRNA nanoparticles by in-line coupling of asymmetrical-flow field-flow fractionation with small angle X-ray scattering. *Sci. Rep.* **2023**, *13* (1), 15764.
(64) Spinozzi, F.; Moretti, P.; Perinelli, D. R.; Corucci, G.; Piergiovanni, P.; Amenitsch, H.; Sancini, G. A.; Franzese, G.; Blasi, P. Small-angle X-ray scattering unveils the internal structure of lipid nanoparticles. *J. Colloid Interface Sci.* **2024**, *662*, 446−459.
(65) Shimokawa, N.; Hamada, T. Physical Concept to Explain the Regulation of Lipid Membrane Phase Separation under Isothermal Conditions. *Life* **2023**, *13* (5), 1105.
(66) Zhang, W.; Pfeifle, A.; Lansdell, C.; Frahm, G.; Cecillon, J.; Tamming, L.; Gravel, C.; Gao, J.; Thulasi Raman, S. N.; Wang, L.; et al. The Expression Kinetics and Immunogenicity of Lipid Nanoparticles Delivering Plasmid DNA and mRNA in Mice. *Vaccines* **2023**, *11* (10), 1580.
(67) Ci, L.; Hard, M.; Zhang, H.; Gandham, S.; Hua, S.; Wickwire, J.; Wehrman, T.; Slauter, R.; Auerbach, A.; Kenney, M.; et al. Biodistribution of Lipid 5, mRNA, and Its Translated Protein Following Intravenous Administration of mRNA-Encapsulated Lipid Nanoparticles in Rats. *Drug Metab. Dispos.* **2023**, *51* (7), 813−823.

https://doi.org/10.1021/acsami.5c06464
ACS Appl. Mater. Interfaces 2025, 17, 28012−28024